Bottom-up isotropization in classical statistical lattice gauge theory

Sebastian Scheffler (TU Darmstadt)

Santa Barbara, February 26, 2008

(In collaboration with J. Berges and D. Sexty)

Reference: arXiv:0712.3514 [hep-ph], to be published in PRD

Outline of the talk

Outline of the talk

RHIC physics & plasma insabilities

- Ideal hydrodynamics applicable at RHIC for $p_T \lesssim 1.5 - 2$ GeV, starting from early times $\tau \lesssim 1$ fm/c (Heinz, AIP Conf. Proc. 739)
- Requires rapid isotropization (Arnold et al., PRL 94)
- Plasma instabilities have been suggested as process that can provide fast isotropization

$\Rightarrow$ **Understanding the early applicability of hydrodynamics means understanding fast isotropization due to plasma instabilities.**

RHIC physics & plasma insabilities

- Ideal hydrodynamics applicable at RHIC for $p_T \lesssim 1.5 - 2$ GeV, starting from early times $\tau \lesssim 1$ fm/c (Heinz, AIP Conf. Proc. 739)
- Requires rapid isotropization (Arnold et al., PRL 94)
- Plasma instabilities have been suggested as process that can provide fast isotropization

$\Rightarrow$ **Understanding the early applicability of hydrodynamics means understanding fast isotropization due to plasma instabilities.**

Numerical approaches:

1. Soft classical gauge fields + hard classical particles (Arnold, Moore, Yaffe; Rebhan, Romatschke Strickland; Dumitru, Nara, Strickland; Bödeker, Rummukainen)
2. Classical statistical gauge field evolution (Romatschke, Venugopalan; this work)

Outline of the talk

Approach

Setup:

- Classical statistical limit of pure SU(2)- gauge theory
- Static geometry, i. e. no expansion
- Lattice discretization of the fields
- Anisotropic initial conditions

Classical statistical approximation reliable for high occupation numbers (Aarts, Berges, PRL 88; Arrizabalaga, Smit, Tranberg, JHEP 0410; Berges, Gasenzer, PRA 76)

Implementation

Use common lattice discretization scheme

Link variables: $U_{x,\mu} := e^{igaA_\mu(x)}$

Plaquette variables: $U_{x,\mu\nu} := U_{x,\mu} U_{(x+\hat{\mu}),\nu} U^{-1}_{(x+\hat{\nu}),\mu} U^{-1}_{x,\nu}$

Dynamics from Wilson- lattice action in Minkowski- spacetime:

$$S = \beta_s \sum_x \sum_{\substack{i,j \\ i<j}} \left\{ \frac{1}{2\mathrm{tr}\mathbb{1}} \mathrm{tr}\left(U_{x,ij} + U^\dagger_{x,ij}\right) - 1 \right\} - \beta_0 \sum_x \sum_i \left\{ \frac{1}{2\mathrm{tr}\mathbb{1}} \mathrm{tr}\left(U_{x,0i} + U^\dagger_{x,0i}\right) - 1 \right\}$$

where

$$\beta_0 := \frac{2\gamma \mathrm{tr}\mathbb{1}}{g_0^2}\ ,\ \beta_s := \frac{2\mathrm{tr}\mathbb{1}}{\gamma g_s^2}\ ,\ \gamma := \frac{a_s}{a_t}$$

We use temporal axial gauge $A_0 \equiv 0$ and $g_0 = g_s = 1$.

Variation w. r. t. spatial links $\Rightarrow$ Equations of motion

Initial conditions

Compute physical quantities (e. g. correlators) according to

$$\langle A(t,\mathbf{x})A(t',\mathbf{y})\rangle = \int \mathcal{D}A(t_0)\,\mathcal{D}\dot{A}(t_0)\,P[A(t_0),\dot{A}(t_0)]\,A(t,\mathbf{x})A(t',\mathbf{y})$$

Initial probability functional $P[A(t_0),\dot{A}(t_0)]$:

$$\langle A^a_j(0,\mathbf{p})A^b_k(0,-\mathbf{p})\rangle \sim C\delta^{ab}\delta_{jk}\exp\{-\frac{p_x^2+p_y^2}{2\Delta_x^2}-\frac{p_z^2}{2\Delta_z^2}\}\,\delta(\dot{A}(t_0))$$

N.B.:

- $\Delta_x \gg \Delta_z$ (distribution $\delta(p_z)-$ like on the lattice)
- $\partial_t\mathbf{A}(t=0)\equiv 0 \;\Rightarrow$ Gauss constraint fulfilled
- Amplitude C determined from fixed average energy density ϵ

Outline of the talk

1. RHIC physics & plasma instabilities
2. Classical statistical gauge theory on the lattice
3. Numerical results
4. Conclusions & Summary

Characteristic time scales (I)

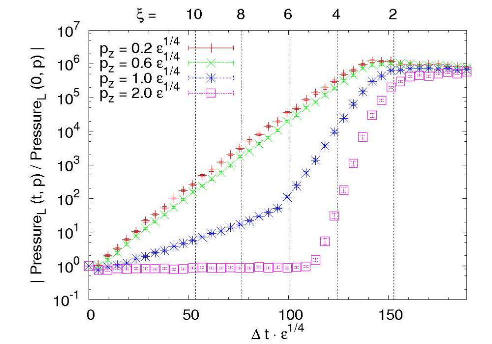

$$T_{33}(t,\mathbf{x}) = \frac{1}{2a_s^4 g^2}\Big\{\gamma^2\Big(\big(1-\frac{1}{2}\operatorname{tr} U_{x,01}\big) + \big(1-\frac{1}{2}\operatorname{tr} U_{x,02}\big) - \big(1-\frac{1}{2}\operatorname{tr} U_{x,03}\big)\Big)$$
$$+ \big(1-\frac{1}{2}\operatorname{tr} U_{x,23}\big) + \big(1-\frac{1}{2}\operatorname{tr} U_{x,31}\big) - \big(1-\frac{1}{2}\operatorname{tr} U_{x,12}\big)\Big\}$$

$\rightsquigarrow$ Fourier transform w. r. t. $\mathbf{x}$ and obtain $T_{33}(t,\mathbf{p})$.

Characteristic time scales (I)

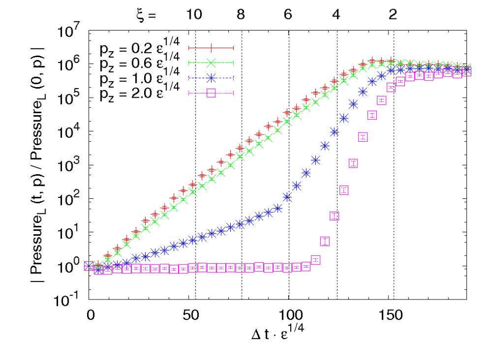

$$\xi(t) := \log_{10}\left\{ \frac{\frac{1}{2}\sum_{\mathbf{p}}(p_x^2+p_y^2)\left(\sum_{j=1}^{3}\sum_{a=1}^{3}|A_j^a(t,\mathbf{p})|^2\right)}{\sum_{\mathbf{q}} q_z^2\left(\sum_{k=1}^{3}\sum_{b=1}^{3}|A_k^b(t,\mathbf{q})|^2\right)} \right\}$$

Characteristic time scales (I)

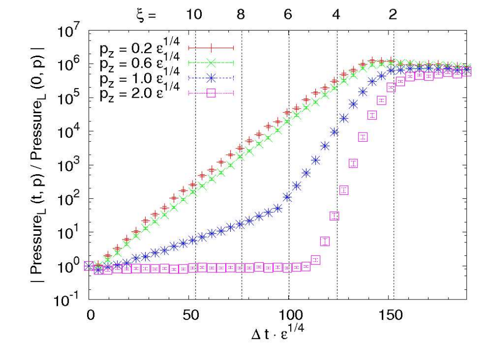

- Narrow band of low-momentum modes unstable initially: *primary instabilities*
- Later, fast growth in a broad range in the UV: *secondary instabilities*
- Findings qualitatively similar to parametric resonance in scalar field theory
- Inverse growth rates yield characteristic time scales

Characteristic time scales (II)

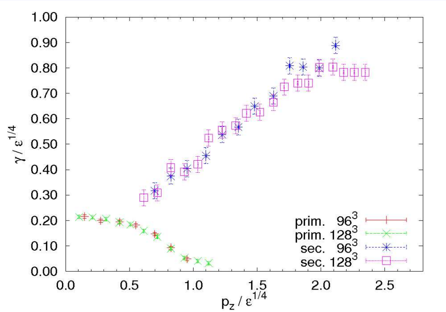

Inverse maximum growth rates (for $|A(t,\mathbf{p})|^2$):

ϵ	$1/\gamma_{\max}^{(pr)}$	$1/\gamma_{\max}^{(sec)}$
30 GeV/fm^3	1.0 fm/c	0.3 fm/c
1 GeV/fm^3	2.6 fm/c	0.8 fm/c

Characteristic time scales (II)

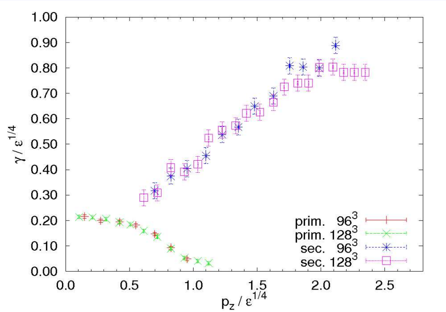

Inverse maximum growth rates (for $|A(t,\mathbf{p})|^2$):

ϵ	$1/\gamma_{max}^{(pr)}$	$1/\gamma_{max}^{(sec)}$
30 GeV/fm^3	1.0 fm/c	0.3 fm/c
1 GeV/fm^3	2.6 fm/c	0.8 fm/c

Obtain $\gamma^{-1} \sim \mathcal{O}(1\ \text{fm/c})$ for primary instabilities

$1/\gamma_{max}^{(pr)} = 0.1$ fm/c would require unrealistic $\epsilon \sim 300$ TeV/fm^3

'Bottom-up isotropization'

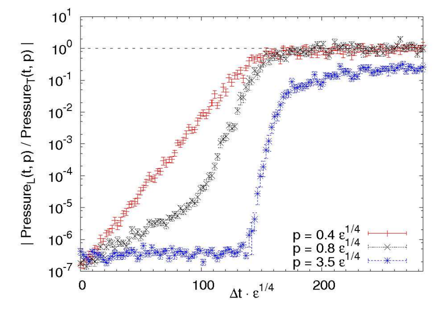

Plotted is

$$\left|\frac{T_{33}(t,\mathbf{p}_{||})}{T_{\perp}(t,\mathbf{p}_{\perp})}\right|_{|\mathbf{p}_{||}|=|\mathbf{p}_{\perp}|}$$

versus time.

- Instabilities drive the system towards an isotropic state
- IR- regime ($p \lesssim \epsilon^{1/4} \simeq 1\,\mathrm{GeV}$) quickly becomes isotropic
- The UV-sector only isotropizes at very late times when the approach cannot be trusted anymore.

'Bottom-up isotropization'

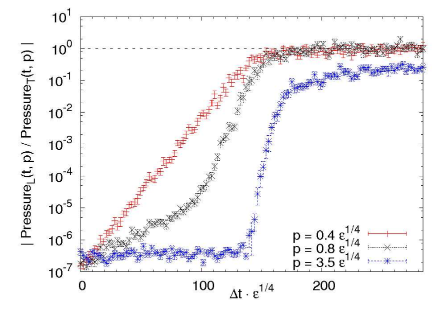

Plotted is

$$\left|\frac{T_{33}(t,\mathbf{p}_{||})}{T_{\perp}(t,\mathbf{p}_{\perp})}\right|_{|\mathbf{p}_{||}|=|\mathbf{p}_{\perp}|}$$

versus time.

- Instabilities drive the system towards an isotropic state
- IR- regime ($p \lesssim \epsilon^{1/4} \simeq 1\,\mathrm{GeV}$) quickly becomes isotropic
- The UV-sector only isotropizes at very late times when the approach cannot be trusted anymore.

$\rightsquigarrow$ "bottom-up isotropization"

Diagramatic analysis of secondaries (I)

Correlation function $F^{ab}_{\mu\nu}(x,y) := \langle\, A^a_\mu(x) A^b_\nu(y)\,\rangle$ obeys a 2PI-evolution equation:

$$[D_0^{-1}]^\gamma_\mu F_{\gamma\nu}(x,y) = \int_{t_0}^{x^0} dz \Pi^\gamma_{(\rho)\mu}(x,z)\, F_{\gamma\nu}(z,y) - \int_{t_0}^{y^0} dz \Pi^\gamma_{(F)\mu}(x,z)\, \rho_{\gamma\nu}(z,y)$$

$(\rho : -\text{Poisson bracket})$ (Berges, PRD 70)

Try to identify times when certain diagrams make $\mathcal{O}(1)$- contributions to the correlation function $F^{ab}_{\mu\nu}(x_0, y_0, \mathbf{p})$ in analogy to parametric resonance in scalar theories (Berges and Serreau, PRL 91) .

Diagramatic analysis of secondaries (I)

Correlation function $F^{ab}_{\mu\nu}(x,y) := \langle\, A^a_\mu(x) A^b_\nu(y) \,\rangle$ obeys a 2PI-evolution equation:

$$[D_0^{-1}]^\gamma_\mu F_{\gamma\nu}(x,y) = \int_{t_0}^{x^0} dz \Pi^\gamma_{(\rho)\mu}(x,z)\, F_{\gamma\nu}(z,y) - \int_{t_0}^{y^0} dz \Pi^\gamma_{(F)\mu}(x,z)\, \rho_{\gamma\nu}(z,y)$$

(ρ : $-$Poisson bracket) (Berges, PRD 70)

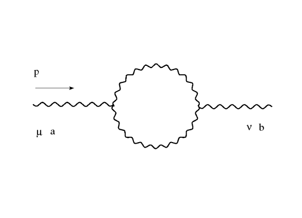

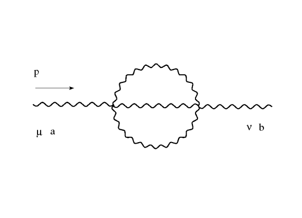

Diagramatic analysis of secondaries (II)

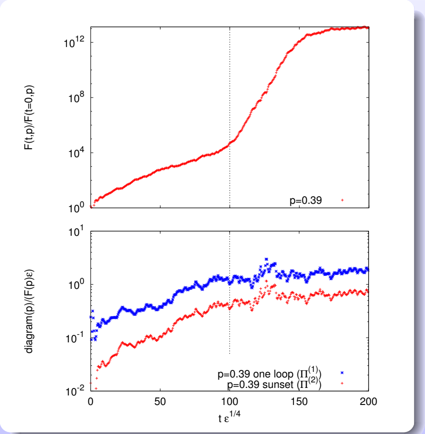

Upper panel:

$$F(t,t,\mathbf{p})/F(t=0,t'=0,\mathbf{p})$$

Lower panel:

$$\left| \frac{\text{diagram}(t,t,\mathbf{p})}{F(t,t,\mathbf{p})\cdot\epsilon} \right|$$

Same $\mathbf{p}\,||\,\hat{z}$ chosen in both panels.

Diagramatic analysis of secondaries (II)

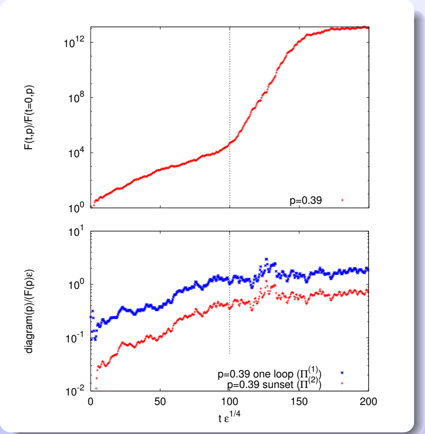

Upper panel:

$$F(t,t,\mathbf{p})/F(t=0,t'=0,\mathbf{p})$$

Lower panel:

$$\left| \frac{\text{diagram}(t,t,\mathbf{p})}{F(t,t,\mathbf{p})\cdot\epsilon} \right|$$

Onset of secondaries coincides with fluctuation effects becoming large, analogous to parametric resonance in scalar theories.

Time evolution of spatial Wilson loops

$t = 5\epsilon^{-1/4}$

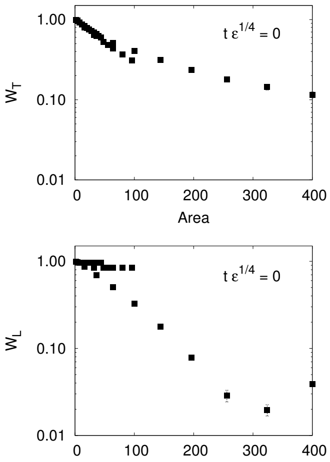

- Initially, area law in the transverse plane only
- Later, longitudinal loops obey an area law, too.
- Spatial string tension $\sqrt{\kappa}$ becomes isotropic
- $\sqrt{\kappa} \to 0.14\,\epsilon^{1/4}$ at late times
- Expect $\kappa \neq 0$ in equilibrium (Manousakis, Polonyi, PRL 58)

Time evolution of spatial Wilson loops

$t = 20\epsilon^{-1/4}$

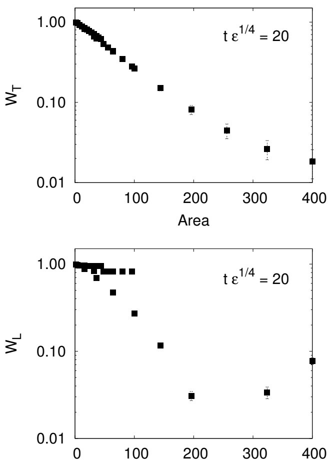

- Initially, area law in the transverse plane only
- Later, longitudinal loops obey an area law, too.
- Spatial string tension $\sqrt{\kappa}$ becomes isotropic
- $\sqrt{\kappa} \to 0.14\,\epsilon^{1/4}$ at late times
- Expect $\kappa \neq 0$ in equilibrium (Manousakis, Polonyi, PRL 58)

Time evolution of spatial Wilson loops

$t = 160\epsilon^{-1/4}$

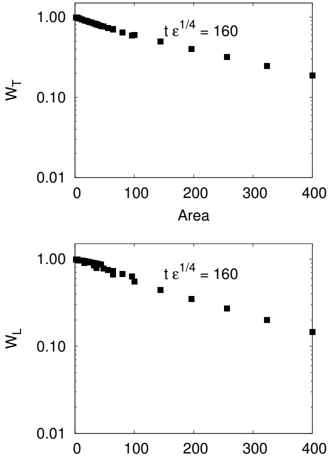

- Initially, area law in the transverse plane only
- Later, longitudinal loops obey an area law, too.
- Spatial string tension $\sqrt{\kappa}$ becomes isotropic
- $\sqrt{\kappa} \to 0.14\,\epsilon^{1/4}$ at late times
- Expect $\kappa \neq 0$ in equilibrium (Manousakis, Polonyi, PRL 58)

Outline of the talk

Conclusions & Summary

- Characteristic time scales of plasma instabilities:

$$1/\gamma_{\mathrm{max}} \sim 1\ \mathrm{fm/c}$$

- 'Bottom-up isotropization' of the IR- sector

$$p \lesssim 1\ \mathrm{GeV}$$

- UV- sector remains anisotropic till late times

Is this sufficient for hydrodynamics?

Are quantum corrections important for the UV-modes?

Thanks for your attention.

Appendix: Volume and cutoff independence

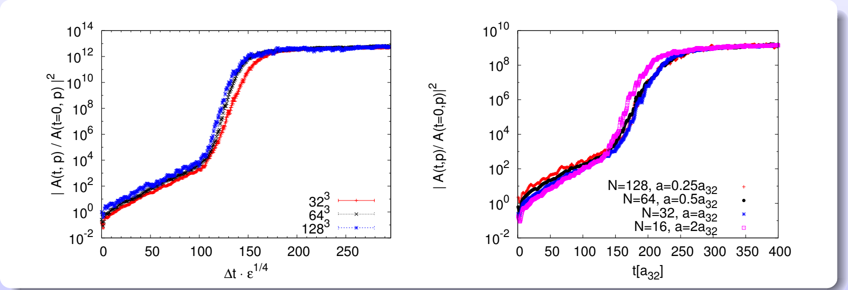

Checking for possible volume and cutoff sensitivities of the results.